HHS Public Access

Author manuscript

Sci Signal. Author manuscript; available in PMC 2020 April 21.

Published in final edited form as:

Sci Signal. ; 13(619): . doi:10.1126/scisignal.aay0086.

Fluoride exposure alters Ca^{2+} signaling and mitochondrial function in enamel cells

Francisco J. Aulestia[1], **Johnny Groeling**[1], **Guilherme H. S. Bomfim**[1], **Veronica Costiniti**[1], **Vinu Manikandan**[2], **Ariya Chaloemtoem**[2], **Axel R. Concepcion**[3], **Yi Li**[1], **Larry E. Wagner II**[4], **Youssef Idaghdour**[2], **David I. Yule**[4], **Rodrigo S. Lacruz**[1,*]

[1]Department of Basic Science and Craniofacial Biology, New York University College of Dentistry, New York, NY 10010, USA.

[2]Biology Program, Division of Science and Mathematics, New York University Abu Dhabi, Abu Dhabi, United Arab Emirates.

[3]Department of Pathology, New York University School of Medicine, New York, NY 10016, USA.

[4]Department of Pharmacology and Physiology, University of Rochester, Rochester, NY 14526, USA.

Abstract

Fluoride ions are highly reactive, and their incorporation in forming dental enamel at low concentrations promotes mineralization. In contrast, excessive fluoride intake causes dental fluorosis, visually recognizable enamel defects that can increase the risk of caries. To investigate the molecular bases of dental fluorosis, we analyzed the effects of fluoride exposure in enamel cells to assess its impact on Ca^{2+} signaling. Primary enamel cells and an enamel cell line (LS8) exposed to fluoride showed decreased internal Ca^{2+} stores and store-operated Ca^{2+} entry (SOCE). RNA- sequencing analysis revealed changes in gene expression suggestive of endoplasmic reticulum (ER) stress in fluoride- treated LS8 cells. Fluoride exposure did not alter Ca^{2+} homeostasis or increase the expression of ER stress–associated genes in HEK-293 cells. In enamel cells, fluoride exposure affected the functioning of the ER-localized Ca^{2+} channel IP_3R and the activity of the sarco-endoplasmic reticulum Ca^{2+}-ATPase (SERCA) pump during Ca^{2+} refilling of the ER. Fluoride negatively affected mitochondrial respiration, elicited mitochondrial membrane depolarization, and disrupted mitochondrial morphology. Together, these data provide a potential mechanism underlying dental fluorosis.

One-sentence summary:

*Corresponding author: rodrigo.lacruz@nyu.edu.

Author contributions: F.J.A., R.S.L., D.I.Y., and Y.I. designed the project. F.J.A., V.C., G.H.S.B., J.G., L.E.W., Y.L., A.R.C., D.I.Y, and R.S.L. collected the data. F.J.A., V.C., G.H.S.B., J.G., L.E.W., A.R.C., D.I.Y., A.C., V.M., Y.I., and R.S.L. analyzed the data. R.S.L. and Y.I. designed the RNASeq experiment. F.J.A., V.C., G.H.S.B., L.E.W., A.R.C., D.I.Y., Y.I., and R.S.L. wrote the paper.

Competing interests: The other authors declare that they have no competing interests.

Data and materials availability: The RNASeq data have been deposited in NCBI Gene Expression Omnibus (GEO) under the accession number GSE143536. All other data needed to evaluate the conclusions in the paper are present in the paper or the Supplementary Materials.

The mechanisms by which excessive fluoride causes defects in tooth enamel mineralization are revealed.

Editor's Summary:How too much fluoride derails dentition

Excessive fluoride ingestion during childhood results in defective tooth enamel mineralization, which can lead to dental problems later in life. Aulestia *et al.* investigated the molecular mechanisms underlying fluorosis in enamel-forming cells isolated from rats and in an enamel cell line. Exposure of enamel cells to fluoride resulted in decreases in ER Ca^{2+} content and store-operated Ca^{2+} entry into the ER, reduced the expression of genes encoding ER stress–response proteins, and resulted in mitochondrial dysfunction. These effects were not seen in HEK-293 cells (which are derived from kidney epithelium). These data may explain how fluorosis affects Ca^{2+} homeostasis in enamel-forming cells and highlight cell type–specific stress responses.

INTRODUCTION

Fluoride is abundant in the environment, readily ingested, and found in serum at low micromolar concentrations (1). The main sources of fluoride intake are drinking water and toothpaste. When epidemiological studies reported that fluoride intake was an important factor in caries prevention, drinking water was supplemented in many areas of the world (2, 3). Fluoride ions are highly reactive, and their incorporation in dental enamel during the development phase at low concentrations promotes mineralization and decreases the solubility of enamel (3, 4). Enamel formed by fluoroapatite is more resistant to acid attack (5).

Enamel crystals develop in specialized extracellular compartments modulated by the activities of epithelial cells, known as ameloblasts, during the secretory and maturation stages of enamel development (6–8). Ameloblasts coordinate the transport of ions required for the growth of crystal (7, 8). The effects of fluoride incorporation during enamel development are reversed when excessive fluoride intake occurs, posing a health problem known as dental fluorosis (DF) (3, 9, 10). Rather than strengthening the bonds between enamel crystals, excessive fluoride disrupts mineralization, resulting in pitted enamel with white opaque surfaces and hypomineralization (3, 9, 11, 12). DF is exclusively a developmental defect and has a major effect worldwide: ~30% of the U.S. population and ~60 million people in India are affected by DF with varying degrees of severity (2, 13). Therefore, the current recommendation for daily fluoride intake is less than 1.0 ppm (parts per million), with water fluoridation not exceeding 0.7 ppm (0.7 mg/kg) (14).

The mechanisms by which fluoride causes DF are complex. Variables affecting the impact of fluoride include its concentration, duration of exposure, and whether fluoride intake occurs during the formative (or secretory) or mineralizing (or maturation) stages of enamel development (3, 10, 12, 15). It may also have a genetic component given the variable impact of excessive fluoride intake on different mouse strains (16). Fluoride is primarily excreted in urine, which may also affect DF models. DF induction in rodents requires a higher fluoride dosage than in humans, likely because fluoride excretion is faster in rodents (7, 17).

Unlike bone, enamel does not remodel once formed, and there- fore, developmental defects such as DF cannot be reversed, leading to studies of the effects of excessive fluoride intake on the formation of enamel crystals in the extracellular milieu (3, 12, 15, 18). Excess fluoride leads to retention of enamel matrix proteins, irregular crystal formation, and hypomineralization (12, 15, 19–21). Despite decades of research on DF, the cellular mechanisms directly responsible for this disease remain poorly understood (22). In primary enamel cells or cell lines, fluoride causes protein misfolding, induces endoplasmic reticulum (ER) stress, and increases the unfolded protein response (UPR) (23–26). The UPR enables cells to cope with misfolding of proteins in the ER (27, 28). These effects suggest that fluoride could interfere with ER Ca^{2+} concentration ($[Ca^{2+}]_{ER}$), though this has not yet been explored. The ER is the main cellular hub for protein folding, requiring the presence of luminal ER Ca^{2+} ($[Ca^{2+}]_{ER}$) (~500 μM) to allow chaperones to perform their protein-folding functions (29, 30). Thus, disruptions in $[Ca^{2+}]_{ER}$ mediated by fluoride could be a cause for reported protein misfolding and UPR in enamel cells.

Fluoride also affects Ca^{2+} transport because it reduces Ca^{2+} levels in the enamel fluid, the compartment where crystals are formed, of fluoride-treated rats (31). An important modulator of Ca^{2+} homeostasis in enamel cells is store-operated Ca^{2+} entry (SOCE), a mechanism that enables sustained Ca^{2+} influx (32, 33). SOCE is mediated by the ER-localized Ca^{2+} sensors STIM1 and STIM2, which interact with the pore of the ORAI1 to ORAI3 channels found in the plasma membrane (34, 35). The activation of SOCE is initiated after the loss of luminal Ca^{2+} in the ER, stimulating the accumulation of STIM1-forming punctae, a prerequisite for the gating of ORAI1 (36, 37).

These reports on UPR and abnormal Ca^{2+} homeostasis in enamel cells suggest a possible connection between fluoride exposure and abnormal ER Ca^{2+}. Here, we address these questions, focusing on the possible interaction of fluoride with molecular elements associated with Ca^{2+} signaling and homeostasis in the cell membrane and endomembranes. We report that fluoride-treated enamel cells showed abnormal ER Ca^{2+} loading and up-regulation of ER stress markers, in part because the refilling of ER by SERCA (sarco-endoplasmic reticulum Ca^{2+}–adenosine triphosphatase) was affected. Fluoride disrupted the activity of inositol 1,4,5-trisphosphate receptor (IP_3R) and affected cellular bioenergetics. RNA-sequencing (RNASeq) analysis revealed that fluoride affected LS8 and human embryonic kidney (HEK)–293 cells differently. These data provide a mechanism on the intracellular effects of fluoride in enamel cells, which help to explain the molecular mechanisms that cause DF.

RESULTS

Enamel cells, but not HEK-293 cells, show low Ca^{2+} after fluoride treatment

To investigate the possibility that fluoride affects Ca^{2+} homeostasis in enamel cells, we isolated rat primary enamel organ (EO) cells from secretory and maturation stages as described previously (38, 39). Because primary EO cells are notoriously difficult to maintain in culture (6, 40), we also used the well-known ameloblast cell line, LS8 cells (41), and HEK-293 cells. Cells were treated for 24 hours with NaF (1 mM) before they were loaded with the cytosolic Ca^{2+} dye Fura-2 AM (1 μM). We used 1 mM NaF (~19 ppm) because

dose-response experiments showed that LS8 cells exposed at 1 mM had the greatest defects in peak release and SOCE (fig. S1). This concentration is higher than fluoride levels in serum (~8 μM), but serum [F^-] can rise several fold once fluoride is ingested including through the consumption of water with ppm values higher than those used here (42–44). Moreover, 1 mM NaF has been reported to cause cell stress in enamel cells in vitro (26) and affects rat incisor enamel in vivo (45). The internal Ca^{2+} stores were depleted passively using the SERCA inhibitor thapsigargin (1 μM) or tBHQ (5 μM) (2,5-di-*tert*-butyl- 1,4-benzohydroquinone) before external Ca^{2+} containing Ringer solution was re-added to stimulate SOCE, as previously described (32). Cells exposed to thapsigargin or tBHQ (5 μM) showed similar release kinetics (fig. S2). After SERCA inhibition, all three enamel cell types (secretory, maturation, and LS8) showed lower internal Ca^{2+} and SOCE compared to control cells, effects not seen in HEK-293 cells (Fig. 1, A to F). These data combined indicate that the effects of fluoride on internal Ca^{2+} stores and SOCE are not generalized features in all cells because only enamel cells were affected.

Fluoride, but not bromide or chloride, affects [Ca^{2+}] in enamel cells

To directly determine the effects of fluoride on $[Ca^{2+}]_{ER}$, we measured $[Ca^{2+}]_{ER}$ with the genetically encoded ER-targeted Ca^{2+} indicator R-CEPIA1-er in cells treated with NaF. Depletion of ER Ca^{2+} by thapsigargin resulted in loss of Ca^{2+} after 30 min of stimulation, with additional decreases 1 and 2 hours after treatment (Fig. 2A). We analyzed $[Ca^{2+}]_{ER}$ in secretory cells because these cells are abundant in ~4-week-old rat incisors. Analysis with the ER Ca^{2+} probe Mag-Fura-2 revealed a decrease in ER Ca^{2+} levels after NaF incubation (Fig. 2B). To determine whether physiological agonists such as adenosine triphosphate (ATP) could mobilize Ca^{2+} from internal stores in fluoride-treated cells, we transiently stimulated Fura-2 AM-loaded LS8 cells with ATP after incubation with NaF but measured only a small response (fig. S3). Together, these data suggest that fluoride decreases ER Ca^{2+} pools in enamel cells.

Because of the unusual effects of fluoride on [Ca^{2+}], we next asked whether other anions would induce similar responses in LS8 cells. NaBr (1 mM) did not elicit changes in ER Ca^{2+} release or SOCE after 1 or 24 hours of exposure (Fig. 2, C to F). Similarly, treatment with NaCl (1 mM) did not affect ER Ca^{2+} or SOCE (fig. S4). These data suggest that fluoride was responsible for changes in ER Ca^{2+} release and SOCE in enamel cells.

RNASeq analysis identifies distinct effects of fluoride in HEK-293 and enamel cells

Because LS8 and HEK-293 cells showed different responses to fluoride treatment, we used RNASeq to analyze global patterns of gene expression changes and pathways involved in this response. We first performed a flow cytometry analysis of annexin V–positive cells, which did not show an increase in cell death in fluoride-treated LS8 cells after 24 hours (fig. S5).

RNASeq analyses identified 2743 differentially expressed genes [DEGs; false discovery rate (FDR) < 1%] in fluoride-treated LS8 cells and 1723 DEGs (FDR < 1%) in HEK-293 cells (Fig. 3, A and B, and tables S1 and S2). Because fluoride exposure can have detrimental and stressful effects on cells, we analyzed the DEGs to determine whether ER stress and the

UPR were induced, as is the case when $[Ca^{2+}]_{ER}$ is abnormally low (1, 17, 28, 46). Genes encoding factors associated with cell stress and UPR were up-regulated in LS8 cells (Fig. 3C) but not in HEK-293 cells (fig. S6), as was also confirmed by quantitative real-time polymerase chain reaction (qRT-PCR) (Fig. 3D and fig. S7). Numerous genes encoding factors involved in the biogenesis of the mitochondrial complexes I, II, and V and coenzyme Q were significantly down-regulated (FDR < 1%) (Fig. 3E) together with mitochondrial ribosomal proteins (MRPs), with 35 MRP elements out of 78 down-regulated (Fig. 3F and table S1). Mitochondrial ribosomes (mitoribosomes) contain 78 genes in the family (MRPL-long; MRPS-short) and almost exclusively synthesize the protein complexes of the respiratory chain (47). The expression of *Stim1*, *Stim2*, or *Orai* genes was not changed in fluoride-treated LS8 cells, but *Saraf* (which encodes store-operated Ca^{2+} entry–associated regulatory factor, a negative modulator of SOCE) was up-regulated (table S1).

In contrast, HEK-293 showed extensive down-regulation (~4% of 1723 DEGs) in genes encoding factors associated with the biogenesis of ribosomal proteins (RPs), with ~82% (66 of 80) small subunit (SSU) or large subunit (LSU) RPs significantly down-regulated (FDR < 1%) (fig. S8 and table S2). RPs are key components of ribosome biogenesis, and they are a limiting rate in protein translation. Humans have 47 LSU RPs and 33 SSU RPs (48). This large-scale down-regulation of the RPs of the LSU and SSU in HEK-293 cells suggests suppression of protein translation, thus preventing UPRs because it averts an increase in misfolded proteins. Similar to LS8 cells, the expression of *STIM1*, *STIM2*, or *ORAI* genes did not change, but in contrast, *SARAF* expression was down-regulated (table S2).

IP_3Rs mediate ER Ca^{2+} release in enamel cells in a manner altered by fluoride

Low Ca^{2+} ER content in fluoride-treated enamel cells suggests that the release mechanism of ER Ca^{2+} or SERCA-mediated refilling might have been affected. Our previous work reported that the inositol receptors (IP_3Rs) were the likely ER Ca^{2+} release channels in LS8 and primary enamel cells (38, 49), although this conclusion was based on gene and protein expression patterns of the IP_3R subtypes. Using two approaches, we analyzed whether IP_3Rs were functional channels in enamel cells. First, saponin-permeabilized primary secretory and maturation and LS8 cells loaded with the ER Ca^{2+} dye Mag-Fura-2 were stimulated with IP_3 (100 nM), which resulted in a marked drop in ER Ca^{2+} content (Fig. 4, A to C). To confirm these results by a different approach in intact cells, we loaded secretory EO cells simultaneously with caged IP_3 and the cytosolic Ca^{2+} dye Fluo-8, as previously reported (50). Secretory EO cells were stimulated with two pulses of ultraviolet (UV) light to uncage IP_3, resulting in increased $[Ca^{2+}]_{cyt}$ (fig. S9). These data indicate that enamel cells express functional IP_3Rs.

As expected, IP_3 uncaging in fluoride-treated secretory EO cells did not elicit changes in $[Ca^{2+}]_{cyt}$ (fig. S9), suggesting that fluoride affects ER Ca^{2+} release by modulating IP_3Rs. To determine the speed at which fluoride affected IP_3Rs, we loaded permeabilized LS8 cells with Mag-Fura-2 and transiently stimulated the cells with NaF. Neither of the NaF concentrations used (10 μM and 1 mM) mobilized ER Ca^{2+} pools (Fig. 4D), suggesting that the effects of fluoride on IP_3Rs did not occur immediately. Similarly in intact cells, transient application of various concentrations of NaF failed to elicit changes in $[Ca^{2+}]_{cyt}$ (fig. S10, A

to D). To address whether fluoride treatment altered the IP_3-IP_3R interaction, we loaded LS8 cells with Mag-Fura-2 to assess the kinetics of the release of IP_3 -sensitive ER Ca^{2+} pools in the presence and absence of fluoride (Fig. 4E). The release rate of IP_3 -sensitive Ca^{2+} pools was significantly faster in untreated control cells than in fluoride-treated cells (for 24 hours) (Fig. 4F). These data suggest that fluoride affects the IP_3 -induced Ca^{2+} release.

ER refilling by SERCA is modified by fluoride

Because $[Ca^{2+}]_{ER}$ depends on the interplay between Ca^{2+} release and refilling by SERCA, we also investigated the refilling capacity of these pumps. We treated LS8 cells with NaF 1 mM (24 hours) and used the reversible SERCA inhibitor tBHQ (5 μM). In saponin-permeabilized, NaF-treated cells, tBHQ depleted ER Ca^{2+} stores. We then switched the solution to an intracellular-like medium to allow ER Ca^{2+} refilling as previously reported (33) to measure the kinetics of ER refilling. Fluoride-treated cells showed slower refilling kinetics by SERCA compared to control cells (Fig. 4, G and H) without changes in SERCA2 abundance (fig. S11), indicating that, in addition to its effects on ER Ca^{2+} release, fluoride also affected SERCA activity.

Fluoride alters mitochondrial Ca^{2+} function and morphology

Because RNASeq analyses of fluoride-treated LS8 cells revealed down-regulation of mitochondrial genes, we further investigated the effects of fluoride on mitochondria. Stimulation of Rhod-2–loaded (2 μM) LS8 cells with ATP resulted in a marked increase in mitochondrial Ca^{2+} (Fig. 5A). Although fluoride-treated cells were able to take up Ca^{2+} in mitochondria under the same conditions, this increase was diminished compared to untreated cells (Fig. 5A). Because fluoride affects the mitochondrial membrane potential (51), we analyzed this effect in LS8 and in primary secretory EO cells loaded with the fluorescent probe TMRM (tetramethylrhodamine methyl ester) to monitor the membrane potential of mitochondria. Transient application of the protonophore FCCP (carbonyl cyanide-*p*-trifluoromethoxyphenylhydrazone) or fluoride depolarized mitochondria in LS8 and in primary secretory EO cells (Fig. 5, B and C). We next determined the potential effects of fluoride on mitochondrial function by measuring oxygen consumption rate (OCR), an indicator of mitochondrial respiration (52), in LS8 cells treated with NaF for 4 hours, a time period that minimized cell detachment during experimental manipulations and during which initial effects of NaF could be detected (Fig. 2A). Compared to control cells, fluoride pretreatment resulted in decreased basal and maximal respiration and in decreased ATP turnover rate (Fig. 5D). We next investigated the ultrastructural characteristics of mitochondria in fluoride-treated cells by transmission electron microscopy (TEM). In many of these cells, mitochondria showed the presence of white, non–electron-dense matrix spaces and a lack of cristae compared to control cells (Fig. 5, E to G). Together, these data indicate that fluoride affects mitochondrial morphology and function in enamel cells.

Disrupted ETC complexes affect SOCE

Our data above provide a basis for interpreting the effects of fluoride on ER Ca^{2+} homeostasis. However, the reasons why SOCE is also decreased in fluoride-treated cells remains unclear. In some cells, the capacity of mitochondria to sequester Ca^{2+} in their matrix is an important element in the functioning of SOCE (53–55). We found that fluoride

treatment decreased SOCE and $[Ca^{2+}]_{mit}$, although $[Ca^{2+}]_{mit}$ was affected before SOCE was decreased (Fig. 5, H and I). To test whether SOCE is dependent on healthy mitochondria, we measured SOCE in LS8 cells with and without oligomycin and rotenone to disrupt the mitochondrial electron transport chain (ETC) complexes (Fig. 5J). We found that disrupting the ETC complexes markedly decreased SOCE compared to control cells (Fig. 5J and fig. S12), indicating that, in enamel cells, properly functioning mitochondria are required for normal SOCE.

DISCUSSION

Fluoride alters ameloblast function (12), yet the mechanisms associated with DF remain poorly understood despite an increase in DF prevalence (56). Here, we approached the study of DF by analyzing intracellular Ca^{2+} signaling and associated effects in enamel cells exposed to fluoride. Our rationale was based on previous reports of enamel cells treated with fluoride, highlighting ER stress and abnormal protein synthesis (24–26, 57) and low Ca^{2+} concentration in the enamel fluid of fluoride-treated rodents (31). We hypothesized that these effects were caused by abnormal Ca^{2+} homeostasis.

We showed that fluoride treatment resulted in lower intra- cellular Ca^{2+} pools in primary secretory and maturation stage EO cells of rat incisors and in LS8 cells. Furthermore, SOCE was abnormally low in all fluoride-treated enamel cells (Fig. 1, A and B). However, HEK-293 cells did not show alterations in intracellular Ca^{2+} pools after fluoride exposure (Fig. 1D), demonstrating that fluoride does not affect Ca^{2+} homeostasis uniformly. Our data also showed that the internal Ca^{2+} stores affected by fluoride were the ER pools (Fig. 2, A and B). Moreover, cells were not affected by exposure to Br^- or increased Cl^- levels, pointing to F^- as the mediator of changes in Ca^{2+} signaling (Fig. 2, C to F, and fig. S4).

RNASeq analyses provided insight into the processes altered by fluoride. UPR-associated genes were up-regulated in LS8 cells, including *GRP78*, a marker of ER stress (58), likely in response to low ER Ca^{2+}. Our study revealed that mitochondrial-associated processes were affected, as seen by down-regulation of genes associated with mitochondrial biogenesis as well as components of the mitochondrial complexes of the ETC. Seventeen genes encoding factors associated with the biogenesis of NADH (reduced form of nicotinamide adenine dinucleotide) (complex I) and 13 genes encoding ATP synthase (complex V) were down-regulated in LS8 cells (Fig. 3E and table S1), suggesting an attenuation of the mitochondrial respiratory chain. In contrast, the effects of fluoride on HEK-293 cells were dominated by a bulk down-regulation of genes encoding RPs (~82% of all ribosomal genes) (fig. S8 and table S2). The cause of the difference in gene expression changes between LS8 and HEK-293 cells is unclear, although one possibility is that the factors necessary for ribosome biogenesis, which are cell and tissue specific and are correlated with ribosome abundance and the requirements for protein synthesis (59, 60), differ between LS8 and HEK-293 cells. Further work is needed to address this issue.

Fluoride treatment affected $[Ca^{2+}]_{ER}$ in enamel cells, raising at least two possibilities: Fluoride stimulates the release of ER Ca^{2+} or it affects the role of SERCA in the refilling of luminal ER Ca^{2+}. With regard to this first point, we have previously reported that IP_3Rs,

rather than ryanodine receptors, are the likely Ca^{2+} release channels in the ER of enamel cells (38). In the present study, we confirmed that IP_3Rs were active components in ER Ca^{2+} release in permeabilized primary EO and LS8 cells (Fig. 4, A to C) and in intact primary secretory cells (fig. S9).

We found that prolonged treatment but not transient treatment of LS8 cells with fluoride (1 mM or 10 μM) slowed the release of IP_3-sensitive ER Ca^{2+} pools. However, because IP_3 can be stimulated by the activation of G proteins (61) and fluoride stimulates this pathway (62), it is not unreasonable to consider that fluoride stimulated the IP_3-mediated Ca^{2+} release in enamel cells by activating G proteins. Fluoride interactions with G proteins require the presence of Al^{3+}, which results in the formation of AlF_4^-. However, not all G proteins can interact with AlF_4^- (61). As expected, ATP, which stimulates IP_3 production, elicited elevations in $[Ca^{2+}]_{cyt}$ in LS8 cells (fig. S10). However, intact LS8 cells transiently stimulated with various concentrations of fluoride did not show a rise in $[Ca^{2+}]_{cyt}$, suggesting that, in LS8 cells, either fluoride does not stimulate IP_3 production or Al^{3+} is not present in our solutions. If fluoride slows the release of ER Ca^{2+}, how is the $[Ca^{2+}]_{ER}$ so diminished in fluoride-treated cells? $[Ca^{2+}]_{ER}$ results from an interplay between release by IP_3R and refilling by SERCA. Fluoride can interfere with SERCA activity in pancreatic acinar cells (63). Fluoride-treated LS8 cells in which ER Ca^{2+} was depleted showed limited refilling activity, suggesting that fluoride negatively affects the pumping action of SERCA. Over time, this limited action of SERCA could have detrimental effects on ER function.

The tight connections between ER and mitochondria are of interest because disruptions in the flow of Ca^{2+} between these two key organelles can underlie disease pathogenesis (64). We found that stimulation with ATP of fluoride-treated cells resulted in Ca^{2+} up- take by mitochondria, albeit at a significantly decreased amount compared to control cells (Fig. 5A). Because the components of the mitochondrial complexes were down-regulated as shown in the RNASeq analyses (Fig. 3E), we expected a decrease in oxidative phosphorylation. Fluoride-treated LS8 cells showed substantially decreased basal respiration and ATP production after inhibition of the F_o portion of the ATP synthase (complex V) with oligomycin. Maximal respiration elicited by FCCP, which forces H^+ across the inner mitochondrial membrane instead of through the ATP synthase, was also substantially lower in fluoride-treated cells, indicating that fluoride modified cellular bioenergetics. The requirement of ATP for endocytosis (65) may also explain why fluoride affects endocytosis in enamel cells (66) and why fluorosed enamel retains proteins (15). Moreover, we found that transient application of fluoride induced mitochondrial depolarization in LS8 cells. This effect was not as marked as depolarization induced by FCCP, but fluoride moderately modified $\Delta\Psi m$. In addition to these functional defects, TEM micrographs of fluoride-treated LS8 cells demonstrated that many cells and, in many regions of these cells, mitochondria showed non–electron-dense spaces in the matrix, unlike in control cells where most regions of the cells showed mitochondria with well-organized cristae (Fig. 5, E to G).

The data discussed above described the effects of fluoride on ER Ca^{2+} homeostasis. Why SOCE decreased was unclear, although various possibilities can be assessed. The magnitude of SOCE generally correlates with the amount of Ca^{2+} released by the ER. However, we showed that the magnitude in the decrease in ER Ca^{2+} release and SOCE was not

comparable in the three types of enamel cells analyzed (Fig. 1, A to C). Mitochondria contribute to SOCE activity (54, 55, 67), and mitochondrial depolarization decreases SOCE (67). Enamel cells transiently exposed to fluoride showed a decrease in ΔΨm (Fig. 5, B and C). In these cells with disrupted ETC, SOCE was significantly decreased compared to control cells (Fig. 5J), suggesting that healthy mitochondria are important for SOCE in enamel cells. In addition, the up-regulation in NaF-treated LS8 cells of *Saraf*, which encodes a negative modulator of SOCE (68), could also play a role. Last, CRAC channel function is linked with the availability of intracellular ATP (69, 70), and the substantial down-regulation of ATP production in NaF-treated LS8 cells may have also negatively affected SOCE. Together, these data indicate that fluoride may disrupt SOCE by affecting multiple pathways.

In summary, this study investigated how fluoride affected the intracellular milieu of enamel cells. The effects of fluoride were wide ranging and complex. Fluoride affected Ca^{2+} homeostasis but not in all cells. Because transient application of fluoride disrupted ΔΨm but did not immediately affect IP_3 R-mediated ER Ca^{2+} release, we suggest that the dysregulation of Ca^{2+} homeostasis by fluoride in enamel cells is initiated in the mitochondria (Fig. 6). The subsequent disruption of the transmembrane potential for hydrogen ions, which is required for ATP synthesis, results in decreased ATP levels. Such a decrease in ATP limits SERCA function, and as a result, there is a decline in ER Ca^{2+} content. These detrimental defects are compounded by a down-regulation of MRPs. SOCE is attenuated because of low ATP levels, up-regulation of *Saraf*, or mitochondrial dysfunction. Together, our data provide a potential mechanism for DF.

MATERIALS AND METHODS

Cell culture

Primary EO cells were isolated from the lower incisors of Sprague-Dawley rats (100 to 120 g). Secretory and maturation EO cells were isolated as previously described using a molar reference line (38, 39). EO cells were digested with Liberase (0.25 mg/ml; Roche) for 30 min at 37°C, washed in Hanks' balanced salt solution, and plated onto CellTak-coated (Corning) coverslips in X-Vivo15 medium (Lonza) supplemented with 10% fetal bovine serum (FBS), 1% penicillin/ streptomycin, and 1% glutamine. Isolated EO cells were used within 24 hours after dissection. LS8 cells are an immortalized murine- derived enamel cell line (37). LS8 cells were maintained in Dulbecco's modified Eagle's medium (DMEM) supplemented with 10% FBS at 37°C with 5% CO_2.

$[Ca^{2+}]_i$ measurements

Measurements of $[Ca^{2+}]_i$ of single cells were performed as described (32). Briefly, single cells were plated overnight on a round microscope cover glass in X-Vivo15 or DMEM medium supplemented with 10% FBS. Cells were loaded with 1 μM Fura 2-AM for 60 min at room temperature, 1 μM Mag-Fura 2-AM for 60 min at room temperature, or 2 μM Rhod 2-AM for 20 min at 37°C, and washed in Ca^{2+} Ringer solution [2 mM $CaCl_2$, 155 mM NaCl, 4.5 mM KCl, 1 mM $MgCl_2$, 10 mM Na-Hepes, and 10 mM D-glucose (pH 7.4)]. To increase the cell purity in primary EO cells, we labeled fibroblasts using a PE-conjugated

anti-CD90 antibody (1:500 dilution; BioLegend) as described (39) and excluded from further analysis. ER store depletion was stimulated with either 1 μM thapsigargin (Sigma) or 5 μM tBHQ (Sigma) in nominal Ca^{2+}-free Ringer solution, followed by re-addition of 2 mM extracellular Ca^{2+} Ringer solution to stimulate SOCE. Alternatively, SOCE was stimulated by maximally depleting the ER stores with a preincubation for 20 min with thapsigargin (1.25 μM) or tBHQ (5 μM) of Fura-2 AM–loaded (1 μM) cells before re-addition of 2 mM Ca^{2+}. Fluorescence intensities at 510 nm were recorded every 5 s after excitation at 340 and 380 nm for Fura-2 AM or 555 nm for Rhod-2 using a Nikon 2000U Eclipse microscope or a FlexStation III plate reader. The ratio of fluorescence 340 and 380 values correlating with $[Ca^{2+}]_i$ were calculated and graphed.

Cell death

Analysis of cell viability was performed with the APC Annexin V Apoptosis Detection Kit (BioLegend) and propidium iodide (PI; Sigma-Aldrich), and staining was performed according to the manufacturer's protocol. Flow cytometry analysis was carried out in an LSRII flow cytometer using FACSDiva software (BD Biosciences), and data were further analyzed with FlowJo (Tree Star). As a positive control for apoptosis induction, cells were treated with 1 μM staurosporine (Tocris) in parallel with NaF treatments.

Cell transfections

LS8 cells were plated overnight on a round microscope cover glass in X-Vivo15 or DMEM medium supplemented with 10% FBS. Cells were washed with Opti-MEM medium (OM; Thermo Fisher) and kept in OM (1 ml). OM was replaced with 800 μl (per well) of transfection reaction [1 μg of er-RedCEPIA plasmid and Lipofectamine 2000 (Invitrogen) with a 1:3 ratio in OM]. The cells were incubated with the transfection mix over 4 hours before switching to DMEM + 10% serum.

IP_3R stimulation

Cells were plated on 25-mm optical borosilicate poly-L-lysine–coated sterile glass covers (Sigma) at 80% confluence and loaded with 1 μM Mag-Fura-2AM in Ringer solution for 60 min at 37°C in warm water. For permeabilization, cells were perfused (5 ml/min) with intracellular-like medium containing 130 mM KCl, 1 mM KH_2PO_4, 1 mM $MgCl_2$, 1 mM ATP, 5 mM sodium succinate, 5 mM sodium pyruvate, 20 mM sodium Hepes (pH 7.0), Ca^{2+} buffered at 200 nM (with titrated 0.2 mM EGTA and EGTA-Ca^{2+} solutions), and 0.01 saponin for 1 min. The solution was then switched to the intracellular-like medium without saponin for 3 min to allow ER Ca^{2+} refilling. When the ER refilling reached the steady state (plateau), the IP_3R stimulation was done in the same 200 nM Ca^{2+} medium supplemented with 100 nM IP_3. Fluorescence intensities were recorded as indicated above.

IP_3 uncaging

IP_3 uncaging was performed as described previously (50). Briefly, LS8 and secretory cells were treated with NaF (1 mM) for 24 hours before loading them with the Ca^{2+} indicator Fluo-4 and with a cell-permeable form of caged inositol trisphosphate (ci-IP_3/PM) (Tocris Bioscience), simultaneously, for 30 min. ci-IP_3/PM is a cell mem- brane diffusible

compound that is hydrolyzed by cellular esterases. Once the PM group is removed, ci-IP_3 is liberated from the cage via UV photo-stimulus acting in a similar manner to $InsP_3$ at $InsP_3R$, releasing Ca^{2+}. An additional period of ~30 min was allowed for de- esterification of the dye and cage. Cells were then illuminated at 488 ± 10 nm, and fluorescence was collected through a 525 ± 25–nm band-pass filter and captured using the Till Photonics imaging suite. These traces are displayed as % $\Delta F/F_o$, where F is the recorded fluorescence and F_o is the mean of the initial 10 sequential frames. Photo- lytic release was performed by using a pulsed xenon arc lamp (Till Photonics). A high-intensity (0.5- to 5-ms duration; 80 J) discharge of UV light (360 ± 7.5 nm) was reflected onto the plane of focus by using a DM400 dichroic mirror and Nikon 40× oil immersion objective, 1.3 numerical aperture (NA).

SERCA refilling

Cells were plated as indicated above and loaded with 1 μM Mag-Fura-2AM. For permeabilization, cells were perfused (5 ml/min) with 2 mM Ca^{2+} Ringer solution for 1 min followed by perfusion with 0.01 saponin for 1 min in intracellular-like medium containing 2 mM EGTA plus 5 μM of the reversible SERCA inhibitor tBHQ. To allow ER Ca^{2+} refilling, we switched to intracellular-like medium constaining 130 mM KCl, 1 mM KH_2PO_4,1 mM $MgCl_2$, 1 mM ATP, 5 mM sodium succinate, 5 mM sodium pyruvate, 20 mM sodium Hepes (pH 7.0), and Ca^{2+} buffered at 100 nM (with titrated 0.2 mM EGTA and EGTA-Ca^{2+} solutions). Fluorescence intensities were recorded as indicated above. The initial SERCA pumping speed was calculated as the slope of the refilling after the re-addition of 200 nM Ca^{2+} between the first second after the re-addition and when the plateau of the curve is reached. This parameter was obtained using the mean values.

Real-time PCR

Total RNA was isolated using the RNeasy Micro Kit (Qiagen) as indicated by the manufacturer followed by reverse transcription using the iScript cDNA Synthesis Kit (Bio-Rad). For quantitative real- time PCR, we used the SsoAdvanced Universal SYBR Green qPCR Supermix (Bio-Rad) and performed the experiments in a CFX Connect Thermocycler (Bio-Rad). *Gapdh* was used as a housekeeping gene. Primers for *GRP78* were reported in (32) and were used at a concentration of 0.25 nM. Relative quantification of gene expression was determined by the $2^{-\Delta\Delta CT}$ method unless indicated otherwise.

Western blotting

Samples were transferred to a microcentrifuge tube containing 50 μl of nonreducing SDS–polyacrylamide gel electrophoresis containing protease inhibitors and homogenized before heating at 90°C for 2 min, centrifuged, and loaded on 10% mini gels. Electrophoresis was carried out at 200 V and transferred onto nitrocellulose membrane at 80 V for 1 hour. Blots were blocked overnight in 5% nonfat milk powder (Bio-Rad, no. 170–6404) in tris-buffered saline containing 0.05% Tween (TTBS) at 4°C. Membranes were probed with the SERCA antibody (Abcam) diluted at 1:1000 and actin (1:2000; Santa Cruz Biotechnology) in TTBS for 2 hours at room temperature. Blots were washed in TTBS and incubated in anti-rabbit immunoglobulin G peroxidase conjugate (Sigma, no. A6154) for 1 hour (room temperature), washed, and developed using a 3,3′-diaminobenzidine (DAB) staining kit (Sigma, no.

D0426) in accordance with the manufacturer's instructions. Blots were documented (Bio-Rad ChemiDoc MP) and then incubated with anti–β-tubulin horseradish peroxidase conjugate (Abcam, no. ab21058) diluted 1:2000 at room temperature for 1 hour and developed using the DAB staining kit.

Mitochondrial respiration

We used the Mitochondrial Stress Test Kit (Agilent) to analyze mitochondrial oxygen consumption in LS8 cells following the manufacturer's instructions. Briefly, LS8 cells were seeded 24 hours in an XFe24-well microplate (Agilent) at 2500 cells per well in complete DMEM (10% FBS, 1% penicillin/streptomycin, and 1% glutamine). In parallel, a cartridge plate was hydrated with XF Calibrant (1 ml per well; Agilent) and kept overnight in a non-CO_2 incubator. The following day, XF base medium (Agilent) containing 1 mM sodium pyruvate, 2 mM L-glutamine, and 10 mM glucose (pH7.4) was pre- pared, and cells were washed several times with this medium. Each well was refilled with exactly 500 μl of completed XF base medium, and cells were equilibrated for 1 hour in a non-CO_2 incubator. The ATP synthase inhibitor oligomycin, the mitochondrial uncoupler FCCP, and complex I and III inhibitors (rotenone/antimycin A) were serially added in a Seahorse XFe24 Analyzer. All compounds including oligomycin, FCCP, and rotenone/antimycin A (Agilent) were prepared in stock solutions and loaded into the compound plate. Cell plate and compound plate were loaded into a Seahorse XFe Analyzer, and OCR was analyzed by sequential additions of oligomycin, FCCP, and rotenone/antimycin A. After each run, protein content of each well was analyzed via bicinchoninic acid, and data were normalized before analyzing basal respiration, ATP production, maximal respiration, and respiratory reserve.

Mitochondrial membrane potential

Cells were plated on 25-mm optical borosilicate poly-L-lysine–coated sterile glass covers (Sigma) at 80% confluence and loaded with 60 nM TMRM in Ringer solution for 30 min at 37°C in warm water. To maintain the balance of Nernst, the rest of the solutions that were applied in the experiments contained 20 nM TMRM. Images were obtained using a Nikon Eclipse 2000TE coupled with a light-emitting diode light to stimulate cells at 555 nm.

SOCE measurements after inhibiting ETC

To determine the effects of inhibiting mitochondrial function on SOCE in LS8 cells, we maximally depleted the ER stores by preincubating cells for 20 min with thapsigargin (1.25 μM). Cells were also loaded with Fura 2-AM (1 μM). To disrupt mitochondrial complexes of the ETC, we treated cells for 10 min with rotenone (2 μM) and oligomycin (1 μM) to block complexes I and V, respectively, before the re-addition of 2 mM Ca^{2+} to induce SOCE.

RNASeq data

LS8 and HEK-293 cells were treated with NaF (1 mM) for 24 hours in six-well plates at a density of ~80%. RNA was isolated using the RNeasy Micro Kit (Qiagen). RNA quality and quantity were analyzed on an Agilent Bioanalyzer nano chip. RNASeq libraries were prepared using the TruSeq Stranded mRNA Kit (Illumina), starting from 500 ng of deoxyribonuclease (DNase) I (Qiagen)–treated total RNA, following the manufacturer's

protocol. The amplified libraries (10 PCR cycles) were purified using AMPure beads (Beckman Coulter), quantified with a Qubit 2.0 fluorometer (Life Technologies), and visualized in an Agilent 2200 TapeStation system. The libraries were pooled equimolarly, loaded on an S1100 flow cell, and run as paired-end 50-nucleotide reads on a NovaSeq 6000. Raw paired-end sequencing reads from both human and mouse samples were quality controlled using the FASTQC tool (www.bioinformatics.babraham.ac.uk/projects/fastqc/). Poor-quality reads/bases, adapters, and barcodes were removed from the data using Trimmomatic v0.32 (41, 42). The high-quality reads were aligned to either the human genome reference (Ensembl release 84-GRCh38) or the mouse genome (Ensembl release 95-GRCm38) using the STAR aligner (STAR_2.5.2a) and default parameters. Transcript abundance estimation and differential expression analysis were performed using Cufflinks v2.2.1 and Cuffdiff v2.2.1, respectively. Hierarchical clustering using the Ward method and data visualization were done using JMP Genomics v8 (SAS Institute).

Statistics

Statistical analyses of data were done using Prism7 (GraphPad Software). Normality tests were performed before comparing the means. Two-tailed unpaired Student's *t* test or two-way analysis of variance (ANOVA) was used to compare the means. Where appropriate, post hoc tests were performed (Dunnett's or Tukey's multiple comparisons). Differences with *P* values of <0.05 were considered significant: $*P < 0.05$, $**P < 0.005$, and $***P < 0.001$. For RNASeq differential expression analysis, an FDR (the Benjamini-Hochberg procedure) of 1% was used as threshold for statistical significance.

Supplementary Material

Refer to Web version on PubMed Central for supplementary material.

Acknowledgments:

We thank J. Bartlett for discussions, A. Heguy and P. Meyn (Genome Technology Center, NYU School of Medicine) for the RNASeq preparation, and N. Drou and the NYUAD Bioinformatics Core team for assistance with RNASeq data processing.

Funding: This work was funded by the National Institute of Dental and Craniofacial Research (NIH/NIDCR) (R01DE025639 and R01DE027679 to R.S.L. and R01DE014756 to D.I.Y.). Y.I. was supported by New York University Abu Dhabi research grant AD105. The NYU Genome Technology Center is partially supported by Cancer Center Support grant P30CA016087 at the Laura and Isaac Perlmutter Cancer Center.

REFERENCES AND NOTES

1. Barbier O, Arreola-Mendoza L, Del Razo LM, Molecular mechanisms of fluoride toxicity. Chem. Biol. Interact 188, 319–333 (2010). [PubMed: 20650267]
2. Ajiboye AS, Dawson DR III, Fox CH, Committee ASI, American associationfor dental research policy statement on community water fluoridation. J. Dent. Res 97, 1293–1296 (2018). [PubMed: 30189155]
3. Aoba T, Fejerskov O, Dental fluorosis: Chemistry and biology. Crit. Rev. Oral Biol. Med 13, 155–170 (2002). [PubMed: 12097358]
4. Simmer JP, Fincham AG, Molecular mechanisms of dental enamel formation. Crit. Rev. Oral Biol. Med 6, 84–108 (1995). [PubMed: 7548623]

5. Fejerskov O, Changing paradigms in concepts on dental caries: Consequences for oral health care. Caries Res. 38, 182–191 (2004). [PubMed: 15153687]
6. Lacruz RS, Enamel: Molecular identity of its transepithelial ion transport system. Cell Calcium 65, 1–7 (2017). [PubMed: 28389033]
7. Lacruz RS, Habelitz S, Wright JT, Paine ML, Dental enamel formation and implications for oral health and disease. Physiol. Rev 97, 939–993 (2017). [PubMed: 28468833]
8. Smith CE, Cellular and chemical events during enamel maturation. Crit. Rev. Oral Biol. Med 9, 128–161 (1998). [PubMed: 9603233]
9. Angmar-Mansson B, Whitford GM, Single fluoride doses and enamel fluorosis in the rat. Caries Res. 19, 145–152 (1985). [PubMed: 3857977]
10. DenBesten PK, Biological mechanisms of dental fluorosis relevant to the use of fluoride supplements. Community Dent. Oral Epidemiol 27, 41–47 (1999). [PubMed: 10086925]
11. DenBesten P, Li W, Chronic fluoride toxicity: Dental fluorosis. Monogr. Oral Sci 22, 81–96 (2011). [PubMed: 21701193]
12. Bronckers ALJJ, Lyaruu DM, DenBesten PK, The impact of fluoride on ameloblasts and the mechanisms of enamel fluorosis. J. Dent. Res 88, 877–893 (2009). [PubMed: 19783795]
13. Perumal E, Paul V, Govindarajan V, Panneerselvam L, A brief review on experimental fluorosis. Toxicol. Lett 223, 236–251 (2013). [PubMed: 24050947]
14. Department of Health US and Human Services Federal Panel on Community Water Fluoridation, U.S. Public Health Service recommendation for fluoride concentration in drinking water for the prevention of dental caries. Public Health Rep 130, 318–331 (2015). [PubMed: 26346489]
15. Robinson C, Connell S, Kirkham J, Brookes SJ, Shore RC, Smith AM, The effect of fluoride on the developing tooth. Caries Res. 38, 268–276 (2004). [PubMed: 15153700]
16. Everett ET, Yin Z, Yan D, Zou F, Fine mapping of dental fluorosis quantitative trait loci in mice. Eur. J. Oral Sci 119 (suppl. 1), 8–12 (2011). [PubMed: 22243220]
17. Buzalaf MAR, Whitford GM, Fluoride metabolism. Monogr. Oral Sci 22, 20–36 (2011). [PubMed: 21701189]
18. Lyaruu DM, Medina JF, Sarvide S, Bervoets TJM, Everts V, Denbesten P, Smith CE, Bronckers ALJJ, Barrier formation: Potential molecular mechanism of enamel fluorosis. J. Dent. Res 93, 96–102 (2014). [PubMed: 24170372]
19. DenBesten PK, Crenshaw MA, The effects of chronic high fluoride levels on forming enamel in the rat. Arch. Oral Biol 29, 675–679 (1984). [PubMed: 6594099]
20. Chen H, Czajka-Jakubowska A, Spencer NJ, Mansfield JF, Robinson C, Clarkson BH, Effects of systemic fluoride and in vitro fluoride treatment on enamel crystals. J. Dent. Res 85, 1042–1045 (2006). [PubMed: 17062747]
21. Riksen EA, Kalvik A, Brookes S, Hynne A, Snead ML, Lyngstadaas SP, Reseland JE, Fluoride reduces the expression of enamel proteins and cytokines in an ameloblast- derived cell line. Arch. Oral Biol 56, 324–330 (2011). [PubMed: 21167474]
22. Bartlett JD, Dwyer SE, Beniash E, Skobe Z, Payne-Ferreira TL, Fluorosis: A new model and new insights. J. Dent. Res 84, 832–836 (2005). [PubMed: 16109993]
23. Suzuki M, Bandoski C, Bartlett JD, Fluoride induces oxidative damage and SIRT1/ autophagy through ROS-mediated JNK signaling. Free Radic. Biol. Med 89, 369–378 (2015). [PubMed: 26431905]
24. Sierant ML, Bartlett JD, Stress response pathways in ameloblasts: Implications for amelogenesis and dental fluorosis. Cell 1, 631–645 (2012).
25. Sharma R, Tsuchiya M, Tannous BA, Bartlett JD, Measurement of fluoride-induced endoplasmic reticulum stress using Gaussia luciferase. Methods Enzymol. 491, 111–125 (2011). [PubMed: 21329797]
26. Sharma R, Tsuchiya M, Bartlett JD, Fluoride induces endoplasmic reticulum stress and inhibits protein synthesis and secretion. Environ. Health Perspect 116, 1142–1146 (2008). [PubMed: 18795154]

27. Corbett EF, Oikawa K, Francois P, Tessier DC, Kay C, Bergeron JJM, Thomas DY, Krause KH, Michalak M, Ca2+ regulation of interactions between endoplasmic reticulum chaperones. J. Biol. Chem 274, 6203–6211 (1999). [PubMed: 10037706]
28. Lin JH, Walter P, Yen TS, Endoplasmic reticulum stress in disease pathogenesis. Annu. Rev. Pathol 3, 399–425 (2008). [PubMed: 18039139]
29. Vincenz-Donnelly L, Hipp MS, The endoplasmic reticulum: A hub of protein quality control in health and disease. Free Radic. Biol. Med 108, 383–393 (2017). [PubMed: 28363604]
30. van Anken E, Braakman I, Versatility of the endoplasmic reticulum protein folding factory. Crit. Rev. Biochem. Mol. Biol 40, 191–228 (2005). [PubMed: 16126486]
31. Crenshaw MA, Bawden JW, Proteolytic activity in embryonic bovine secretory enamel, in Tooth Enamel IV, Fearnhead RW, Suga S, Eds. (Elsevier Science, 1984) pp. 109–113.
32. Eckstein M, Vaeth M, Fornai C, Vinu M, Bromage TG, Nurbaeva MK, Sorge JL, Coelho PG, Idaghdour Y, Feske S, Lacruz RS, Store-operated Ca^{2+} entry controls ameloblast cell function and enamel development. JCI Insight 2, e91166 (2017). [PubMed: 28352661]
33. Eckstein M, Vaeth M, Aulestia FJ, Costiniti V, Kassam SN, Bromage TG, Pedersen P, Issekutz T, Idaghdour Y, Moursi AM, Feske S, Lacruz RS, Differential regulation of Ca2+ influx by ORAI channels mediates enamel mineralization. Sci. Signal 12, eaav4663 (2019).
34. Prakriya M, Lewis RS, Store-operated calcium channels. Physiol. Rev 95, 1383–1436 (2015). [PubMed: 26400989]
35. Putney JW, The physiological function of store-operated calcium entry. Neurochem. Res 36, 1157–1165 (2011). [PubMed: 21234676]
36. Parekh AB, Putney JW Jr., Store-operated calcium channels. Physiol. Rev 85, 757–810 (2005). [PubMed: 15788710]
37. Wu MM, Buchanan J, Luik RM, Lewis RS, Ca2+ store depletion causes STIM1to accumulate in ER regions closely associated with the plasma membrane. J. Cell Biol 174, 803–813 (2006). [PubMed: 16966422]
38. Nurbaeva MK, Eckstein M, Concepcion AR, Smith CE, Srikanth S, Paine ML, Gwack Y, Hubbard MJ, Feske S, Lacruz RS, Dental enamel cells express functional SOCE channels. Sci. Rep 5, 15803 (2015). [PubMed: 26515404]
39. Nurbaeva MK, Eckstein M, Devotta A, Saint-Jeannet JP, Yule DI, Hubbard MJ, Lacruz RS, Evidence that calcium entry into calcium-transporting dental enamel cells is regulated by cholecystokinin, acetylcholine and ATP. Front. Physiol 9, 801 (2018). [PubMed: 30013487]
40. Klein O, Duverger O, Shaw W, Lacruz RS, Joester D, Moradian-Oldak J, Pugach MK, Wright JT, Millar SE, Kulkarni AB, Bartlett JD, Diekwisch TG, DenBesten P, Simmer JP, Meeting report: A hard look at the state of enamel research. Int. J. Oral Sci 9, e3 (2017). [PubMed: 29165423]
41. Chen LS, Couwenhoven RI, Hsu D, Luo W, Snead ML, Maintenance of amelogenin gene expression by transformed epithelial cells of mouse enamel organ. Arch. Oral Biol 37, 771–778 (1992). [PubMed: 1444889]
42. Whitford GM, The metabolism and toxicity of fluoride. Monogr. Oral Sci 16, 1–153 (1996). [PubMed: 8813212]
43. Bronckers ALJJ, Lyaruu DM, Guo J, Bijvelds MJC, Bervoets TJM, Zandieh-Doulabi B, Medina JF, Li Z, Zhang Y, DenBesten PK, Composition of mineralizing incisor enamel in cystic fibrosis transmembrane conductance regulator-deficient mice. Eur. J. Oral Sci 123, 9–16 (2015). [PubMed: 25557910]
44. Taves DR, Normal human serum fluoride concentrations. Nature 211, 192–193 (1966).
45. Denbesten PK, Crenshaw MA, Wilson MH, Changes in the fluoride-induced modulation of maturation stage ameloblasts of rats. J. Dent. Res 64, 1365–1370 (1985). [PubMed: 2416791]
46. Mekahli D, Bultynck G, Parys JB, De Smedt H, Missiaen L, Endoplasmic-reticulum calcium depletion and disease. Cold Spring Harb. Perspect. Biol 3, a004317 (2011). [PubMed: 21441595]
47. Greber BJ, Ban N, Structure and function of the mitochondrial ribosome. Annu. Rev. Biochem 85, 103–132 (2016). [PubMed: 27023846]
48. Xie X, Guo P, Yu H, Wang Y, Chen G, Ribosomal proteins: Insight into molecular roles and functions in hepatocellular carcinoma. Oncogene 37, 277–285 (2018). [PubMed: 28945227]

49. Nurbaeva MK, Eckstein M, Snead ML, Feske S, Lacruz RS, Store-operated Ca2+ Entry Modulates the Expression of Enamel Genes. J. Dent. Res 94, 1471–1477 (2015). [PubMed: 26232387]
50. Wagner II LE, Li W-H, Joseph SK, Yule DI, Functional consequencesof phosphomimetic mutations at key cAMP-dependent protein kinase phosphorylation sites in the type 1 inositol 1,4,5-trisphosphate receptor. J. Biol. Chem 279, 46242–46252 (2004). [PubMed: 15308649]
51. Yan X, Yang X, Hao X, Ren Q, Gao J, Wang Y, Chang N, Qiu Y, Song G, Sodium Fluoride Induces Apoptosis in H9c2 Cardiomyocytes by Altering Mitochondrial Membrane Potential and Intracellular ROS level. Biol. Trace Elem. Res 166, 210–215 (2015). [PubMed: 25707396]
52. Pelletier M, Billingham LK, Ramaswamy M, Siegel RM, Extracellular flux analysisto monitor glycolytic rates and mitochondrial oxygen consumption. Methods Enzymol. 542, 125–149 (2014). [PubMed: 24862264]
53. Parekh AB, Store-operated Ca2+ entry: Dynamic interplay between endoplasmic reticulum, mitochondria and plasma membrane. J. Physiol 547 (Pt. 2), 333–348 (2003). [PubMed: 12576497]
54. Watson R, Parekh AB, Mitochondrial regulation of CRAC channel-driven cellular responses. Cell Calcium 52, 52–56 (2012). [PubMed: 22387012]
55. Hoth M, Fanger CM, Lewis RS, Mitochondrial regulation of store-operated calcium signaling in T lymphocytes. J. Cell Biol 137, 633–648 (1997). [PubMed: 9151670]
56. Suzuki M, Everett ET, Whitford GM, Bartlett JD, 4-Phenylbutyrate mitigates fluoride-induced cytotoxicity in ALC cells. Front. Physiol 8, 302 (2017). [PubMed: 28553235]
57. Suzuki M, Sierant ML, Antone JV, Everett ET, Whitford GM, Bartlett JD, Uncoupling protein-2 is an antioxidant that is up-regulated in the enamel organ of fluoride-treated rats. Connect. Tissue Res 55 (suppl. 1), 25–28 (2014). [PubMed: 25158175]
58. Brostrom MA, Brostrom CO, Calcium dynamics and endoplasmic reticular function in the regulation of protein synthesis: Implications for cell growth and adaptability. Cell Calcium 34, 345–363 (2003). [PubMed: 12909081]
59. Mills EW, Green R, Ribosomopathies: There's strength in numbers. Science 358, eaan2755 (2017).
60. Farley-Barnes KI, Ogawa LM, Baserga SJ, Ribosomopathies: Old concepts, new controversies. Trends Genet. 35, 754–767 (2019). [PubMed: 31376929]
61. Bigay J, Deterre P, Pfister C, Chabre M, Fluoride complexes of aluminium or beryllium act on G-proteins as reversibly bound analogues of the gamma phosphate of GTP. EMBO J. 6, 2907–2913 (1987). [PubMed: 2826123]
62. Mertz LM, Horn VJ, Baum BJ, Ambudkar IS, Calcium entry in rat parotid acini: Activation by carbachol and aluminum fluoride. Am. J. Physiol 258 (4 Pt. 1), C654–C661 (1990). [PubMed: 2333951]
63. Chong SA, Hong SY, Moon SJ, Park JW, Hong JH, An JM, Lee SI, Shin DM, Seo JT, Partial inhibition of SERCA is responsible for extracellular Ca2+ dependence of AlF-4-induced [Ca2+]i oscillations in rat pancreatic. Am. J. Physiol. Cell Physiol 285, C1142–C1149 (2003). [PubMed: 12878491]
64. Pinton P, Mitochondria-associated membranes (MAMs) and pathologies. Cell Death Dis. 9, 413 (2018). [PubMed: 29549303]
65. Schmid SL, Carter LL, ATP is required for receptor-mediated endocytosis in intact cells. J. Cell Biol 111 (6 Pt 1), 2307–2318 (1990). [PubMed: 2126013]
66. Duan X, Mao Y, Wen X, Yang T, Xue Y, Excess fluoride interferes with chloride-channel-dependent endocytosis in ameloblasts. J. Dent. Res 90, 175–180 (2011). [PubMed: 21148016]
67. Singaravelu K, Nelson C, Bakowski D, de Brito OM, Ng SW, di Capite J, Powell T, Scorrano L, Parekh AB, Mitofusin 2 regulates STIM1 migration from the Ca2+ store to the plasma membrane in cells with depolarized mitochondria. J. Biol. Chem 286, 12189–12201 (2011). [PubMed: 21220420]
68. Jha A, Ahuja M, Maléth J, Moreno CM, Yuan JP, Kim MS, Muallem S, The STIM1 CTID domain determines access of SARAF to SOAR to regulate Orai1 channel function. J. Cell Biol 202, 71–79 (2013). [PubMed: 23816623]
69. Chvanov M, Walsh CM, Haynes LP, Voronina SG, Lur G, Gerasimenko OV, Barraclough R, Rudland PS, Petersen OH, Burgoyne RD, Tepikin AV, ATP depletion induces translocation of

STIM1 to puncta and formation of STIM1-ORAI1 clusters: Translocation and re-translocation of STIM1 does not require ATP. Pflugers Arch. 457, 505–517 (2008). [PubMed: 18542992]

70. Innocenti B, Pozzan T, Fasolato C, Intracellular ADP modulates the Ca2+ release-activated Ca2+ current in a temperature-and Ca2+−dependent Way. J. Biol. Chem 271, 8582–8587 (1996). [PubMed: 8621486]

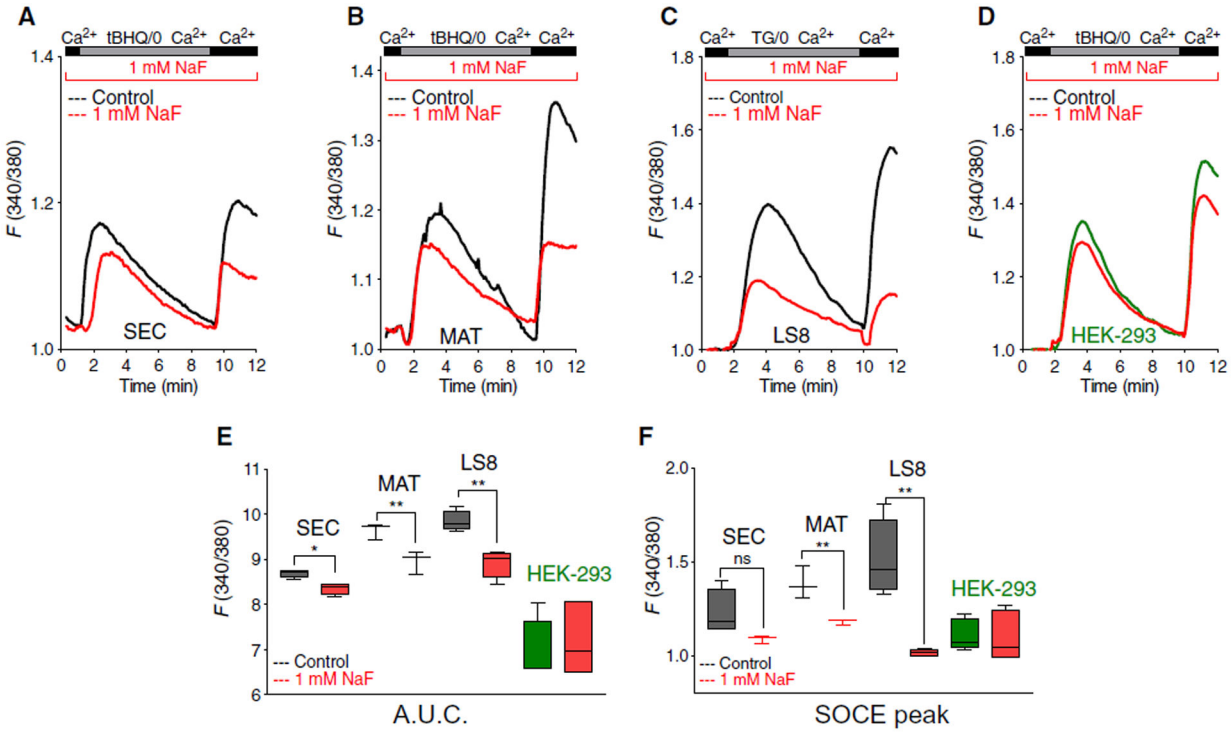

Fig. 1. Fluoride leads to loss Ca^{2+} in internal stores only in enamel cells.

(**A** to **C**) Ca^{2+} levels in internal stores and SOCE upon re-addition of external Ca^{2+} in isolated primary enamel organ (EO) cells from secretory (SEC) (A) and maturation (MAT) (B) stages and LS8 cells (C) incubated with NaF (1 mM) for 24 hours and treated with the SERCA inhibitor thapsigargin (TG) or tBHQ. (**D**) Ca^{2+} levels in internal stores and SOCE upon re-addition of external Ca^{2+} in fluoride-treated HEK-293 incubated with NaF (1 mM) for 24 hours and treated with the SERCA inhibitor tBHQ. (**E** and **F**) Quantification of area under the curve (A.U.C.) (E) (between 2 and 9 min) and peak of SOCE (F) from (A) to (D). Data in (A) and (B) represent the mean ± SEM of three independent experiments analyzed using unpaired Student's *t* test (*$P < 0.01$ and **$P < 0.001$). EO cells were obtained from six rats. Data in (C) and (D) represent the mean ± SEM of four to six independent experiments using unpaired Student's *t* test (**$P < 0.001$); ns, nonsignificant.

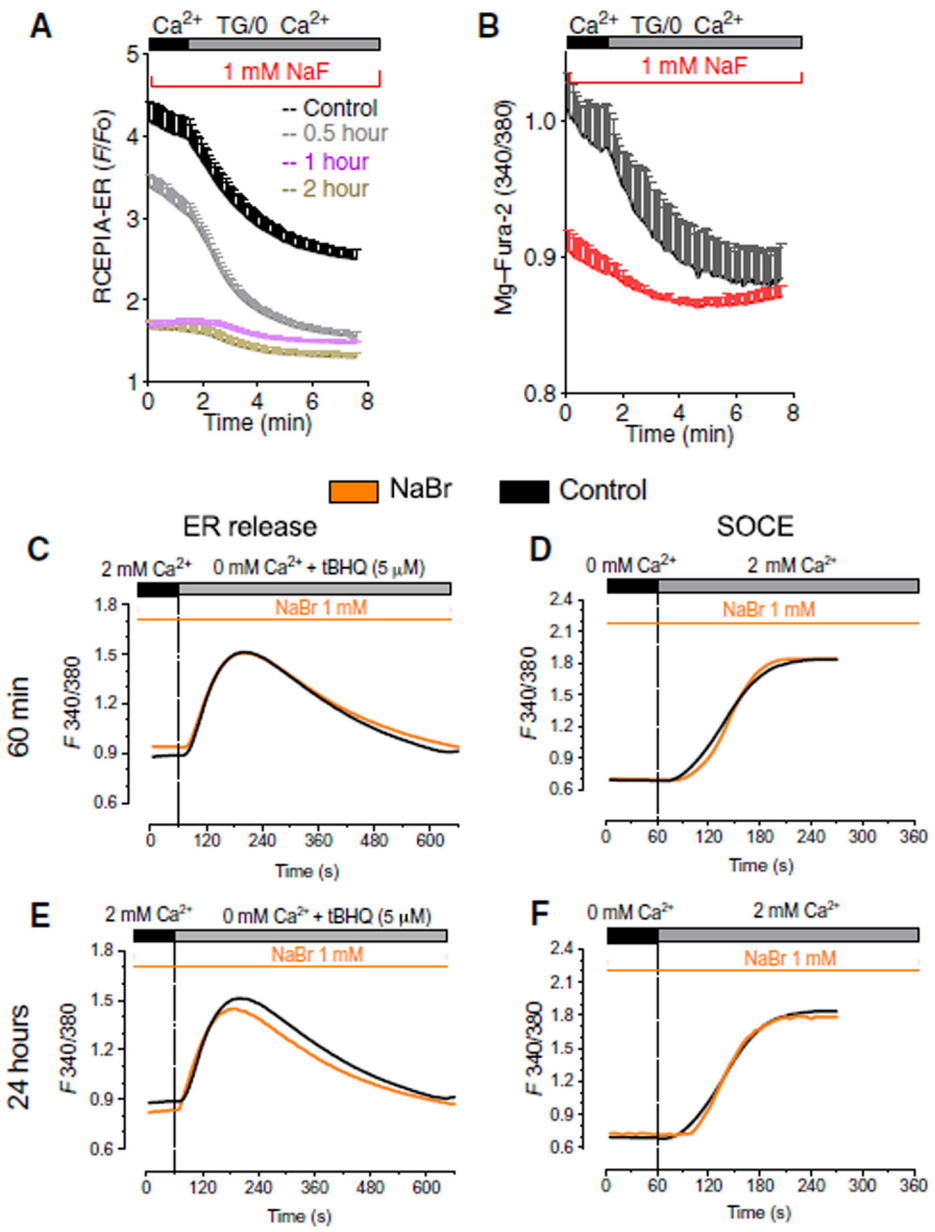

Fig. 2. Fluoride, but not bromide, affects ER Ca^{2+}.

(**A**) ER Ca^{2+} in LS8 cells transfected with the genetically encoded ER Ca^{2+} probe CEPIA-red stimulated with thapsigargin and exposed to fluoride for 30 min (gray trace), 1 hour (blue trace), and 2 hours (green trace). Data represent the mean ± SEM of three independent experiments analyzed using Dunnett's multiple comparisons test (** $P < 0.001$) of 30 min, 1 hour, and 2 hours compared to controls. (**B**) ER Ca^{2+} in primary secretory cells treated with fluoride (24 hours, 1 mM NaF) loaded with the ER Ca^{2+} probe Mag-Fura-2 and stimulated with thapsigargin. Data represent the mean ± SEM of three independent experiments analyzed using Student's *t* test (black compared to red: *** $P < 0.001$). EO cells obtained from three rats. (**C**) ER Ca^{2+} levels in untreated LS8 cells (black trace) or cells treated for 1 hour with NaBr (1 mM) (orange trace). (**D**) SOCE in untreated LS8 (black trace) or cells

treated with NaBr (1 mM) (orange trace) for 1 hour after maximally depleting the stores with tBHQ (5 μM) before re-addition of 2 mM Ca^{2+}. (**E** and **F**) Same as (C) and (D) with cells treated for 24 hours. Data in (C) to (F) represent the mean ± SEM of three independent experiments.

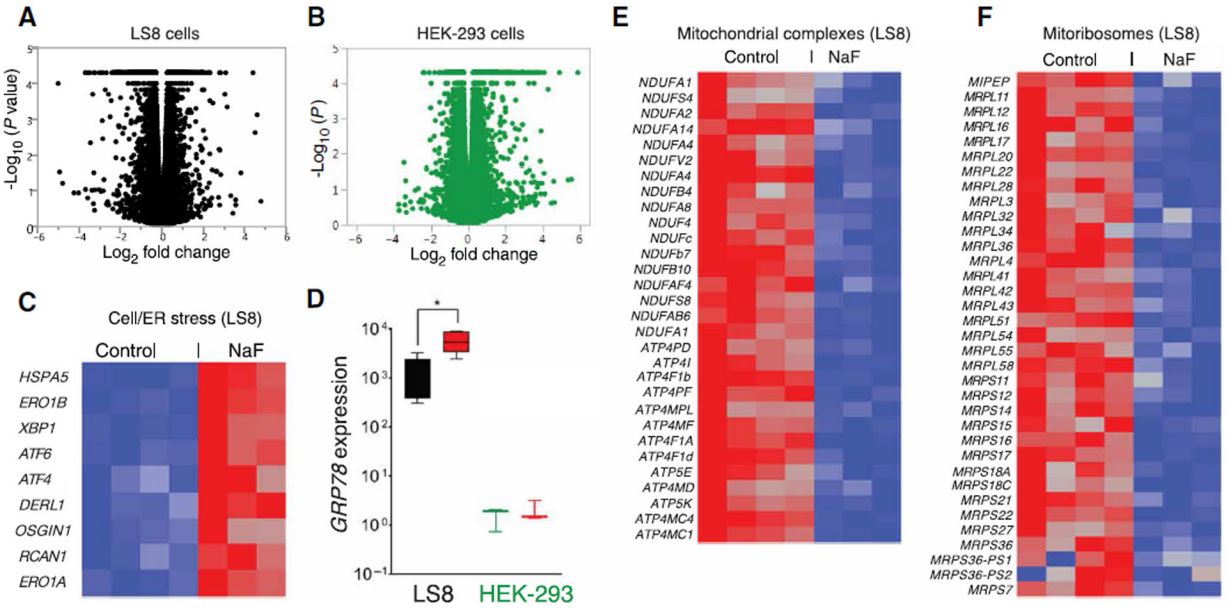

Fig. 3. RNASeq analyses of fluoride-treated LS8 and HEK-293 cells.

(**A** and **B**) Volcano plots of statistical significance (shown as the negative log base 10 of the *P* value on the *y* axis) compared to the magnitude of differential gene expression (shown as the log base 2 of magnitude of mean expression difference on the *x* axis) between control and NaF (1 mM) treatment for murine LS8 (A) and HEK-293 (B) cells. Data in (A) and (B) were obtained from four sets of untreated and three sets of NaF-treated cells. (**C**) Heat map of transcript abundance using one-way hierarchical clustering of untreated and 1 mM NaF–treated LS8 cells for 24 hours, showing the differential expression of genes encoding proteins associated with cell stress and UPR. Red indicates up-regulation. (**D**) RT-PCR showing the mRNA expression of the ER stress marker *GRP78* in LS8 and HEK-293 cells in response to NaF (red boxes). Data represent the mean ± SEM of three independent experiments (**P* < 0.05, ANOVA). (**E**) Differential expression of genes encoding proteins associated with the biosynthesis of mitochondrial complexes in LS8 cells. (**F**) Differential expression of genes encoding proteins associated with mitoribosome biosynthesis in HEK-293 cells. (E and F) Blue indicates down-regulation.

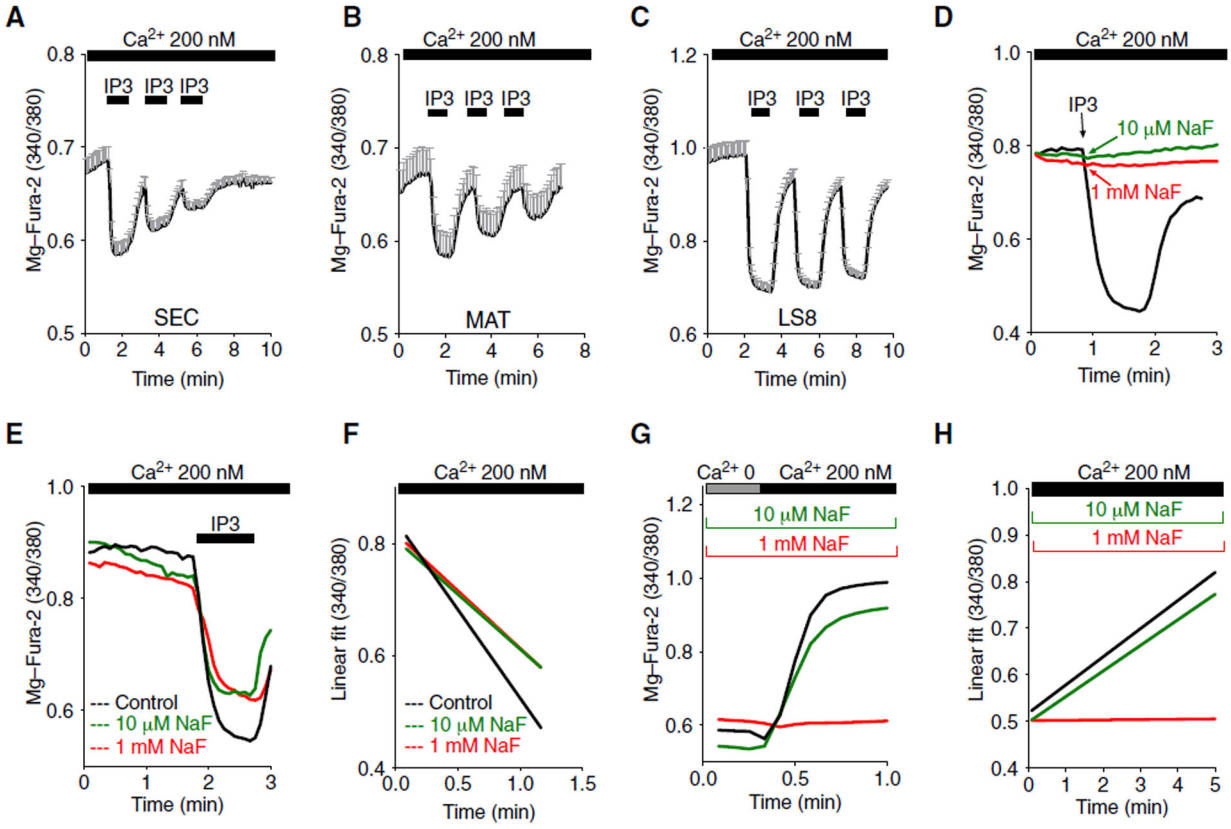

Fig. 4. IP_3R and SERCA functions are modified by fluoride in enamel cells.

(**A** to **C**) Permeabilized LS8 cells (A), primary secretory (B), and maturation (C) stage cells loaded with the ER Ca^{2+} indicator Mag-Fura-2 were stimulated with IP_3 to induce Ca^{2+} release from the ER. Each stimulus resulted in ER Ca^{2+} decrease. Representative tracings of ~100 cells per cell type. (**D**) Release from ER Ca^{2+} pools in permeabilized LS8 cells loaded with the ER Ca^{2+} dye Mag-Fura-2 and transiently stimulated with fluoride at 10 μM (green trace) or 1 mM (red trace). Representative of ~140 cells per group. (**E**) ER Ca^{2+} release by IP_3 stimulation was measured in permeabilized LS8 cells loaded with Mag-Fura-2 pretreated with 10 μM NaF (green trace) and 1 mM NaF (red trace). Representative of ~140 cells per group. (**F**) Kinetics of release from ER Ca^{2+} pools in cells in (E). Data represent the mean ± SEM of three independent experiments using Tukey's multiple comparisons test (black compared to red: $^{**}P < 0.0001$; black compared to green: $^{**}P < 0.001$; red compared to green: ns). (**G** and **H**) Kinetics of SERCA refilling measured in permeabilized untreated LS8 cells after tBHQ stimulation (black trace) and exposure to NaF (10 μM; green trace, and 1 mM; red trace). Data represent the mean ± SEM of three independent experiments using Tukey's multiple comparisons test (black compared to red: $^{****}P < 0.0001$; black compared to green: $^{*}P < 0.0235$; red compared to green: $^{****}P < 0.0001$).

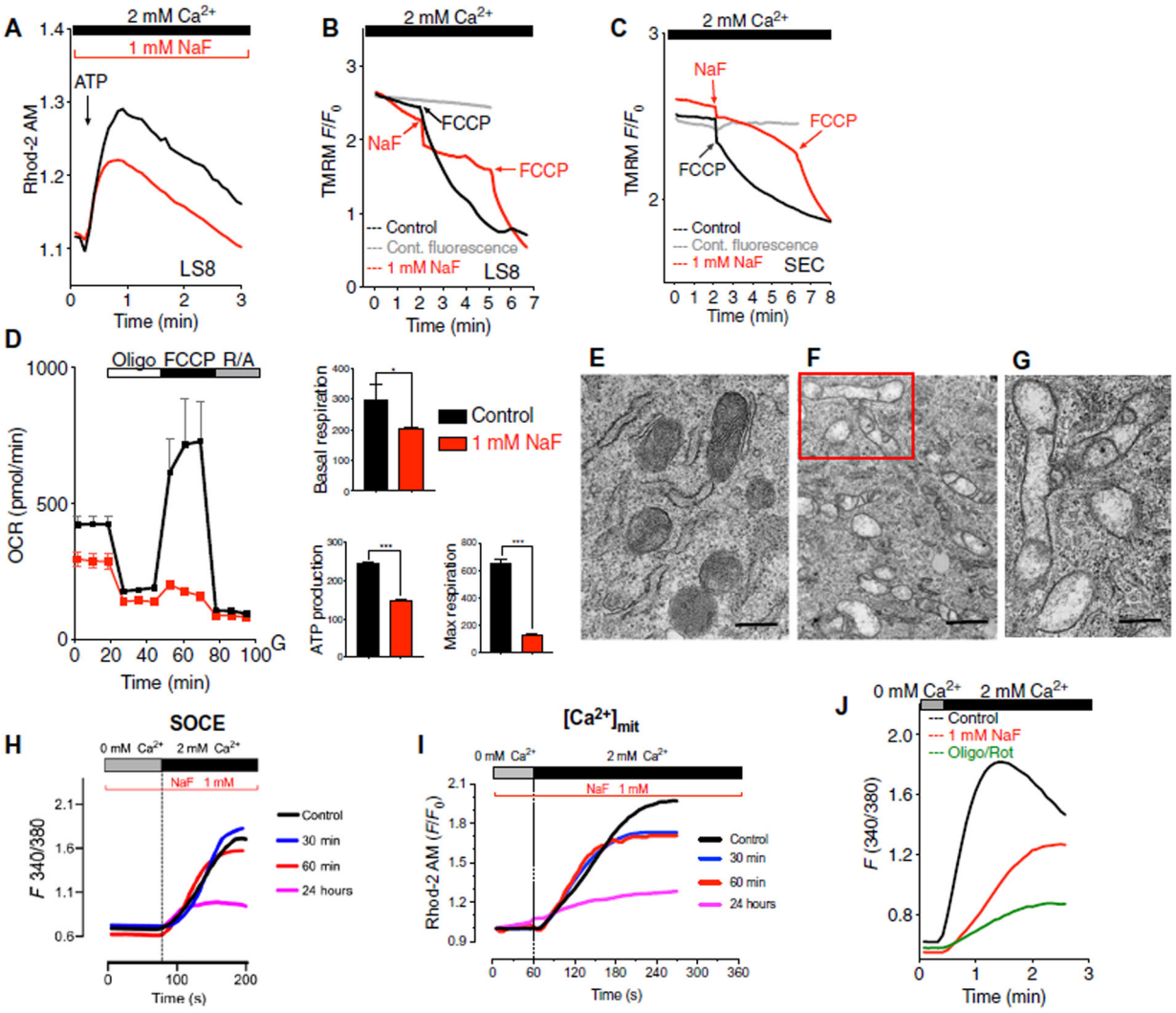

Fig. 5. Fluoride modified mitochondrial function and SOCE.

(**A**) Rhod-2–loaded control (untreated), LS8 (black trace), and fluoride-treated (24 hours) (red trace) cells transiently stimulated with ATP. Data represent the mean ± SEM of three independent experiments using Student's *t* test (black compared to red: ****$P < 0.0001$). (**B**) Mitochondrial membrane potential measured in LS8 cells loaded with TMRM that were untreated and stimulated with FCCP (1.5 μM; black trace) or transiently stimulated with fluoride (1 mM) and FCCP (red trace). TMRM fluorescence was also monitored in cells not treated with FCCP (gray traces). Representative of 150, 100, and 120 cells. (**C**) Primary secretory cells analyzed as in (B). Representative of 90 untreated and stimulated with FCCP (black traces), 65 fluoride-and FCCP-treated cells (red traces), and 80 untreated cells (gray traces). (**D**) Oxygen consumption rate (OCR), basal respiration, ATP production, and maximal respiration in LS8 cells after 4 hours of NaF (1 mM) pretreatment. Data represent the mean ± SEM of three independent experiments using Student's *t* test. (*$P < 0.05$ and ***$P < 0.001$). (**E** to **G**) Transmission electron micrographs of control LS8 cells (E) and fluoride-treated cells (F) (1 mM, 24 hours). Close-up of mitochondria (G) from (F) showing mitochondrial matrix with non–electron-dense matrix lacking cristae. Scale bars, 1 μm (E

and F) and 0.5 μm (G). (**H**) SOCE measured after treating cells for 20 min with thapsigargin in untreated LS8 cells (black trace) or cells treated with NaF (1 mM) after 30 min, 60 min, and 24 hours. (**I**) $[Ca^{2+}]_{mit}$ measured in Rhod-2–loaded LS8 cells after stimulation of SOCE as in (A). (**J**) SOCE measured after treating cells for 20 min with thapsigargin in untreated LS8 cells (black trace) or fluoride-treated (1 mM) cells (red trace) and cells treated with oligomycin (1 μM) and rotenone (2 μM) (green trace). Data in (H) to (J) represent the mean ± SEM of three independent experiments.

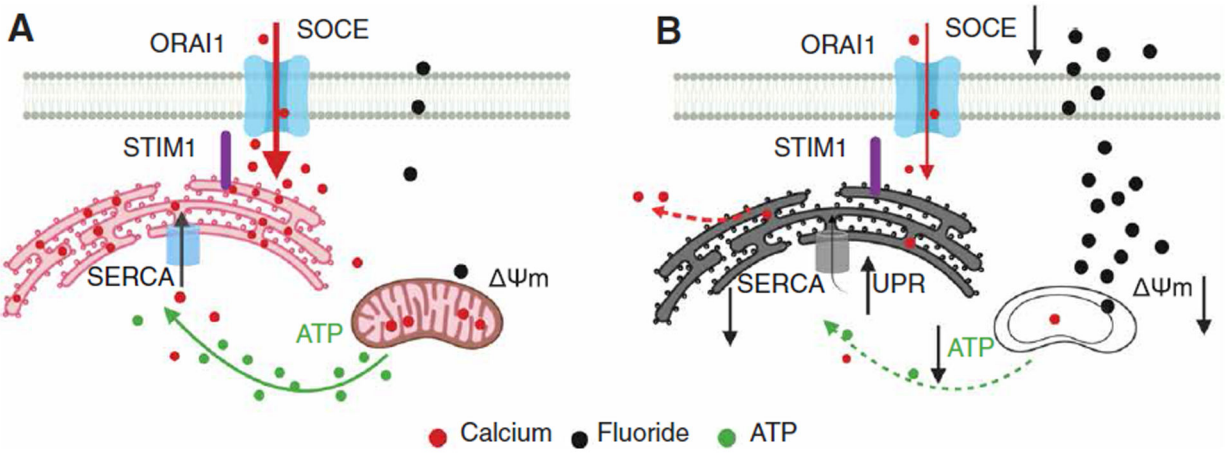

Fig. 6. Model for the effects of high fluoride in enamel cells.

(**A**) In a healthy cell exposed to low fluoride, mitochondrial membrane potential (ΔΨm) and ATP production are normal, enabling SERCA to maintain its pumping function. SOCE is normal. (**B**) High fluoride exposure results in a decrease in the ΔΨm disrupting the proton motive force required to generate ATP. Decreased levels of ATP limit the capacity of SERCA to transfer Ca^{2+} into the ER lumen, resulting in increased Ca^{2+} leak. Cells respond by activating the UPR that allows the cells to survive, albeit in a low metabolic state. SOCE may be decreased because of low ATP or dys-functional mitochondria.